PHOTONICS Research

Anomalous plasmon coupling and Fano resonance under structured light

Da-Jie Yang,[1,2,*] Song-Jin Im,[3,5] Hai-Wen Huang,[1] Chol-Song Ri,[3] Kum-Dong Kim,[3] Kil-Song Song,[3] Ji-Cai Liu,[1,2] and Qu-Quan Wang[4,6]

[1]Mathematics and Physics Department, North China Electric Power University, Beijing 102206, China
[2]Hebei Key Laboratory of Physics and Energy Technology, North China Electric Power University, Baoding 071000, China
[3]Department of Physics, Kim Il Sung University, 02-381-4410 Pyongyang, Republic of Korea
[4]Department of Physics, Southern University of Science and Technology, Shenzhen 518055, China
[5]e-mail: sj.im@ryongnamsan.edu.kp
[6]e-mail: qqwang@sustech.edu.cn
*Corresponding author: djyang@ncepu.edu.cn

Received 22 February 2023; revised 30 March 2023; accepted 13 April 2023; posted 26 May 2023 (Doc. ID 488215); published 1 August 2023

Structured light carrying orbital angular momentum (OAM) opens up a new physical dimension for studying light–matter interactions. Despite this, the complex fields created by OAM beams still remain largely unexplored in terms of their effects on surface plasmons. This paper presents a revelation of anomalous plasmon excitations in single particles and plasmon couplings of neighboring nanorods under OAM beams, which are forbidden using non-OAM sources. The plasmon excitation of single nanoparticles is determined both by photon spin angular momentum (SAM) and OAM and influenced by the locations of the nanoparticles. Specifically, when SAM and OAM are equal in magnitude and opposite in direction, a pure plasmon excitation along light propagation direction is achieved. Two plasmon dipoles show end-to-end antibonding coupling and side-by-side bounding coupling, which are the opposite of the typical couplings. Furthermore, we observe Fano resonance with a nanorod dimer: one aligned along light propagation direction acting as the bright mode and the other aligned along the global polarization direction of light acting as the dark mode, which is the opposite of the usual plasmonic Fano resonance. By taking advantage of the unique property of the OAM source, this investigation presents a novel way to control and study surface plasmons, and the research of plasmon behavior with OAM would open new avenues for controlling electromagnetic waves and enriching the spectroscopies with more degrees of freedom.

https://doi.org/10.1364/PRJ.488215

1. INTRODUCTION

Plasmonic nanostructures, which attracted extensive studies in the past decades, enable unparalleled manipulation of electromagnetic waves at the nanoscale [1–3]. Metallic nanoparticles can exhibit strong modulation of visible light due to the large optical cross section induced in the far field and the strong local field enhancement in the near field by surface plasmons when resonantly excited. Such modulation relies on the resonance modes and couplings of local surface plasmons. Compared with dielectric nanoparticles whose multipole electric and magnetic resonances can be selectively excited and tuned, plasmonic resonances rely on the collective oscillation of free electrons, which mainly exhibit electric resonances and demonstrate stronger coupling with light. Local surface plasmon resonances (LSPRs) stimulated by sources without optical orbital angular momentum (OAM) have been intensively studied. Single nanoparticle plasmon excitations involve dipole and multipole electric plasmon mode [4,5], magnetic mode [6,7], standing waves of surface plasmon polariton [2,8,9], toroidal mode [10,11], as well as chiral plasmon mode [12,13]. Complex plasmon excitations by near-field couplings between adjacent plasmonic nanoparticles give rise to more interesting optical phenomena, which have been modeled as in-phase and out-of-phase couplings [14,15], plasmon hybridization [16–18], Fano resonance [19–23], electromagnetically induced transparency [24,25], and charge transfer plasmon [26,27].

In recent years, the rapid development of laser technology has enabled us to explore light–matter interactions with more degrees of freedom. Structured light with specially designed amplitude, distribution, duration, polarization, and phase expands the spectroscopies with more degrees of freedom [28–31]. In particular, the optical vortex includes a new physical dimension of OAM [32–52], besides the better-known spin angular momentum (SAM). While the SAM of light is associated with the helical electrical vectors or the photon spin, the

OAM of light is related to the helical phase structure of the beam or the photon phase distribution. Twisted photons with the phase structure $e^{il\phi}$ carry an OAM of $l\hbar$ per photon, where l is an integer related to the azimuthal topological charge number, ϕ is the azimuthal angle, and $\hbar$ is the Planck constant. The optical OAM dimension with complete and unbounded sets of eigenfunctions not only provides an efficient dimension for optical multiplexing [53–61] but also creates a complex electric field for light–matter interactions [62–66]. OAM beams have been used to rotate and manipulate small particles since more than 25 years ago [67–70]. In an atom or ions, photons carrying OAM enable high-order electron transitions, which are forbidden using only SAM of light due to the lack of angular momentum (AM) required for the transition [63,64]. Fueled by OAM source technology, nanoplasmonics displays a new vitality. In nanoparticles, OAM beams can induce high-order resonances, which typically result from the retardation effect and are themselves rare when the light does not carry OAM [71,72]. The underlying physical mechanism is AM transfer from the photon to the electron. Recently, excitations of surface plasmon multipoles and dark modes by OAM beams have been demonstrated [72–74]. Plasmonic nanoantennas can also show OAM dichroism [75]. In addition, the OAM of light has been used to control the relative oscillation phases of nanoantennas in a nanoarray, and the interference of radiations from each element in the far field contributes an OAM-modulated phased array nanoantenna [76]. The optical responses of plasmonic nano-oligomers have also been analyzed with symmetry-imposed selection rules using group theory [77,78]. Our work reveals the optical property of oligomers from the perspective of coupling of the individual elements. To the best of our knowledge, there are no prior studies that have specifically explored the effect of photon OAM and SAM on plasmon couplings in the near field, especially Fano resonances stimulated by a vortex beam.

In this investigation, we systematically investigate the excitation and coupling of surface plasmons with the OAM physical dimension. Single plasmonic nanoparticle shows different excitations when it is located at different points of the OAM beams. For single particles illuminated on-center of the light beam, the mode multiplicity of the excited plasmon matches the sum of the quantum number of SAM and OAM. When SAM and OAM are equal in magnitude and opposite in direction, there will be a pure longitudinal polarization along the light propagation direction. This investigation provides a quantitative analysis of the longitudinal polarization state under the influence of a vortex beam. When the nanorod is off-center, its polarization direction is determined by the SAM of light, while the OAM of light influences its oscillation phase. Neighboring nanorods under OAM beams show anomalous couplings. Nanorods located end-to-end (side-by-side) symmetrically along the polarization direction of the OAM beams couple out of phase (in phase), and the spectrum peak blueshifts (redshifts), which appears counterintuitive compared with the non-OAM case. Furthermore, plasmonic Fano resonances occur through the coupling between a bright mode of the nanorod along the propagation direction of light and a dark mode of the nanorod perpendicular to the propagation direction. The dark mode and bright mode giving rise to such a Fano resonance are acted by opposite elements using a non-OAM source. The investigation includes an additional OAM physical dimension to the field of plasmonics and proposes different plasmon excitation and coupling properties which are forbidden under non-OAM sources. Such plasmon behaviors enrich nanoplasmonics and may boost its broad applications in optical modulation, sensing, and computation.

2. RESULTS AND DISCUSSION

A. Interplay between OAM and SAM and LSPR of Single Particles under Vortex Beams

It has been demonstrated in experiments that both the SAM and the OAM of light can be transferred to materials. It is easy to accept that optical SAM can cause a particle rotation or polarization around the axis of the particle. Optical OAM can also rotate or polarize a nanoparticle, but around the axis of the optical beam. The schematic illustration of a nanoparticle polarized by an OAM beam in a spin–orbital state of $|\sigma, l\rangle = |-1,1\rangle$ is shown in Fig. 1(a). OAM of a Laguerre–Gaussian (LG) beam is characterized by the helical wavefront in Fig. 1(a) or by the azimuthal phase gradient in Fig. 1(b). Nanoparticles' polarization is determined both by SAM and OAM.

Now we consider a gold nanorod that shows a longitudinal dipole eigenstate around 640 nm and a transverse dipole eigenstate around 505 nm. When the gold nanorod is located on the center of the beam, OAM and SAM polarize the nanorod around the same axis, so the difference of the total AMs possessed by each of the surface plasmons of the initial and final states must equal the sum of SAM and OAM of the absorbed photon. The surface plasmons excited by photons in $|-1,1\rangle$ state will not carry AM. But it does not mean that surface plasmon could not be excited. The optical scatterings of $|-1,1\rangle$ light by a gold nanorod orientated perpendicular to and along the propagating direction of light are compared in Fig. 2. When the

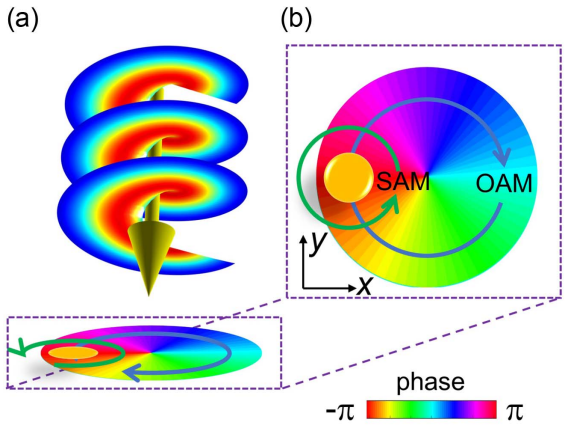

Fig. 1. Interplay between optical OAM and SAM. (a) Schematic illustration of a nanoparticle polarized by an OAM beam with a helical wavefront. (b) Azimuthal phase gradient in the plane transverse to the propagation direction of a vortex beam in a spin-orbital state of $|-1,1\rangle$. The yellow circle schematically refers to the nanoparticle under the illumination of a vortex beam. SAM and OAM induced particle polarizations are indicated by the green arrow and blue arrow, respectively.

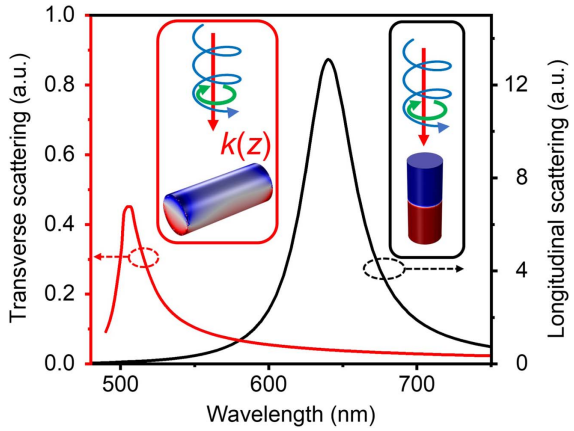

Fig. 2. LSPR of single particles on the center of vortex beams. Optical scatterings of $|\text{-}1,1\rangle$ light by a gold nanorod located on the beam center and orientated perpendicular to (red) and along (black) the propagating direction. The radius and length of the nanorod are 20 nm and 100 nm, respectively. The configurations and surface charge distributions are shown in the insets bordered with the corresponding colors.

nanorod is orientated perpendicular to the propagating direction, only the transverse plasmon mode of the nanorod is excited. The phenomenon is much different from the non-OAM case where both transverse and longitudinal excitations are expected under circularly polarized illumination. When the nanorod is oriented along the propagation direction, the longitudinal plasmon mode of the nanorod is excited. The phenomenon also seems counterintuitive to the non-OAM case, when only transverse is expected. As indicated by the surface charge distributions in the insets, both polarizations are along the propagation direction of the beam. These counterintuitive plasmon behaviors can be understood if we realize the special field profiles of the vortex beams. The local electric field has a component along the propagation direction of the $|\text{-}1,1\rangle$ beam, E_z, as explained in Appendix A. E_z arises from the partial derivatives of the electric field distributions with respect to x and y independently in paraxial approximation. E_z dominates the local polarization of the on-center nanoparticles, which are much smaller than the waist radius of the beam. So, on the focal center of $|\text{-}1,1\rangle$ beams, the plasmon excitation is not along the global polarization direction which defines the overall polarization state of the entire beam, but along the propagation direction of light which is the local polarization direction of the beam. The conclusion also applies to a nanosphere located at the center of an OAM beam or radially polarized beams that have an E_z component [76]. By utilizing an anisotropic nanorod, it is possible to determine in the far field which physical quantity (electric field, magnetic field, or the Poynting vector) governs the polarization of the nanorods. This information can further aid in the investigation of nanorod couplings.

There are four different situations when the nanorod is located off the center of a linearly polarized vortex beam ($|\sigma, l\rangle$ equals $|0,1\rangle$), depending on the orientation and offset directions of the nanorod, as schematically shown in Fig. 3(a). Here, we neglect the discussion of a longitudinally oriented nanorod, whose optical spectrum will hardly show any difference when

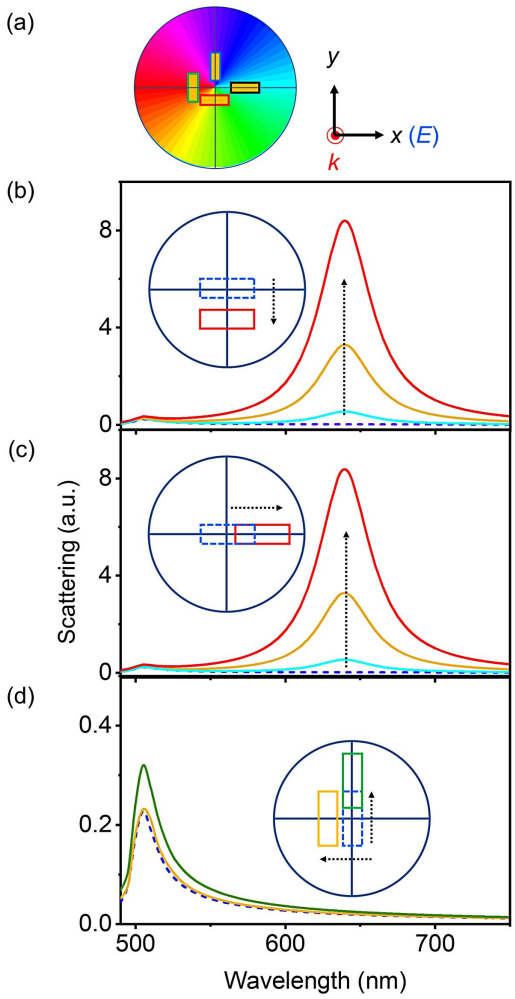

Fig. 3. LSPR of single particles off the beam center of a linearly polarized vortex beam ($|\sigma, l\rangle$ equals $|0,1\rangle$). (a) Four different situations when the nanorod is off-center. The color map shows the phase gradient, and the white arrows show the instantaneous electric field. (b), (c) Optical scatterings of the vortex beam by a nanorod oriented along the polarization direction (E_x) of light and offset along the y and x axes from the center (blue line) by a distance of 20 nm (cyan), 50 nm (yellow line), and 80 nm (red line), respectively. (d) Optical scatterings of the vortex beam by a nanorod oriented along H_y and offset along the y (yellow line) and x axes (green line).

the nanorod is moved within the slowly varying E_z field. When the nanorod is oriented along the electric field (E_x), as shown in Figs. 3(b) and 3(c), an offset from the beam center will "unlock" the longitudinal plasmon mode, and the longitudinal intensity grows when the offset becomes larger. The results can be understood from the perspective of the complex vortical force field. When the nanorod is on the beam center of a linearly polarized vortex beam, the x-z plane divides the nanorod into two identical parts. These two parts suffer equal forces of opposite directions along the electric field (x axis), so the longitudinal plasmon mode is hardly excited. However, when there is an offset, no matter along the x or y axis, there will be a pure electric dipole momentum along the electric field, which grows when the offset becomes larger, and then "unlocks" the longitudinal plasmon mode. When the

nanorod is oriented along the magnetic field H_y, there will be no longitudinal plasmon excitation, no matter whether there is an offset or not. When there is no offset, the transverse plasmon mode is excited by E_z and when there is an offset, the transverse plasmon mode is excited by E_x. To conclude Figs. 3(b)–3(d), when the nanoparticle is on-center, the nanoparticle polarization mode is determined both by OAM and SAM; and when the nanoparticle is off-center, the nanoparticle polarization mode is mainly determined by SAM, while OAM only puts a phase on the polarization.

B. Anomalous Plasmon Couplings under Vortex Beams

Surface plasmons supported by the adjacent nanoparticles will couple through the near field. It has been shown in Figs. 2, 3(b), and 3(c) that longitudinal plasmon modes can be excited when the nanorod is oriented along the light propagation direction or when an off-center nanorod is along the electric field direction of a vortex beam of $|0,1\rangle$. Generally, the couplings of such nanorods depend on the spatial distribution of the nanorods: end-to-end or side-by-side. The spectra of two symmetrically arranged nanorods oriented along the electric field direction are shown in Fig. 4(a). Compared with the spectrum of the single nanorod, the resonance of the end-to-end configuration shows a blueshift, while the resonance of the side-by-side configuration shows a redshift. The corresponding surface charge distributions at the resonance wavelengths are shown in the insets. The two nanorods in the end-to-end configuration oscillate out of phase, resembling an anti-bounding molecular state σ^*, which is at a higher energy level. The oscillation in the side-by-side configuration resembles a bounding molecular state π which is at a lower energy level. Such couplings are exactly the opposite of the non-OAM case, which generally exhibits σ and π^* states. This is because the vortex beam creates a non-uniformly polarized field, which polarizes the two nanorods in opposite directions. The spectra of two nanorods oriented along the propagation direction and stacked side-by-side and end-to-end are shown in Fig. 4(b). The dimer shows a π^* resonance at the high energy level and a σ resonance at the low energy level, which agrees with the non-OAM case. The polarizations of the two nanorods are determined by E_z, which is almost uniform around the nanorod, so the two nanorods oscillate in phase and show a typical plasmon coupling.

C. Anomalous Fano Resonances under Vortex Beams

The couplings of nanorods in different orientations in the x-y plane under an x-polarized vortex beam are shown in Fig. 5. The longitudinal plasmon mode of the nanorod oriented along the electric field direction (x axis) can be excited by the vortex beam when the nanorod is offset from the center. The nanorod oriented along the y axis exhibits no longitudinal excitation, no matter whether the nanorod is offset or not. The configuration of a pair of perpendicular nanorods located at different positions of a vortex beam is schematically shown in Fig. 5(a). The nanorods are moved in the second and fourth quadrants [Fig. 5(a) left] or in the first and third quadrants [Fig. 5(a) right], and their optical scatterings are shown in Figs. 5(b) and 5(c), respectively. The spectra exhibit a Fano line shape:

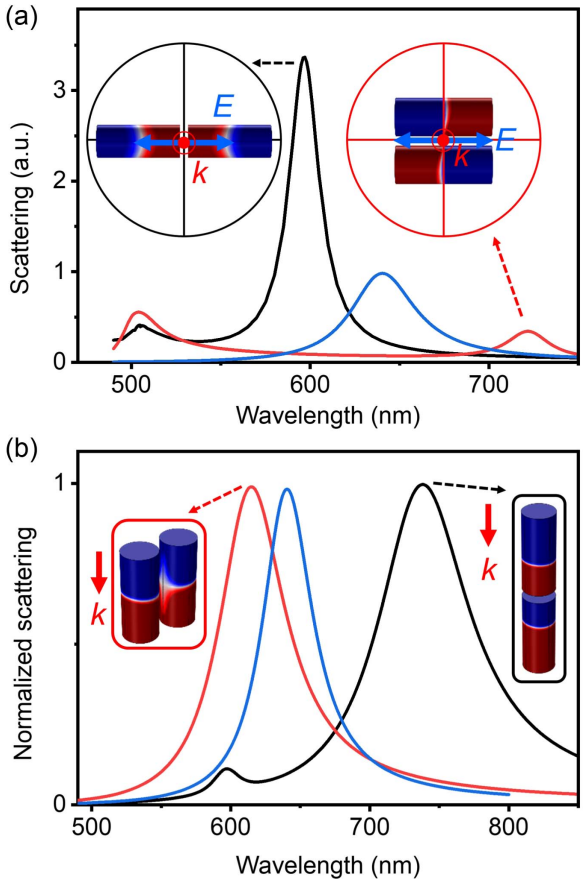

Fig. 4. Anomalous plasmon couplings of two parallel nanorods under vortex beams. Optical spectra of two parallel nanorods located end-to-end (black line) or side-by-side (red line) and oriented (a) along the electric field direction and (b) along the light propagation direction under a linearly polarized vortex beam (l equals 1). The original longitudinal plasmon spectrum of the single nanorod is shown by the blue lines. The insets bordered with black and red show the surface charge distributions at the corresponding peaks. E and k indicate the electric field direction and light propagation direction, respectively.

two peaks divided by a dip at the original resonance wavelength of a single nanorod. The nanorod along the x axis can couple directly with the incident light, while the nanorod along the y axis cannot, as discussed in Fig. 3. So, the nanorods along the x axis and y axis act as the bright mode and dark mode for the Fano resonance, respectively. The phenomenon we observe is the opposite of plasmonic Fano resonance induced by non-OAM beams. In the case of Fano resonance induced by non-OAM beams, the nanorod oriented along the electric field axis behaves as the bright mode, while the nanorod oriented along the propagation direction behaves as the dark mode [20,21]. The surface charge distributions of the nanorods at the two peaks are shown in the insets of Fig. 5(b). At the shorter wavelength, the two nanorods show an out-of-phase state; and at the longer wavelength, the two nanorods show an in-phase state. This further confirms the Fano resonance in the two perpendicular nanorods system under vortex beams. The distribution and relative intensities of the two peaks are not determined by the quadrant where the nanorods are located.

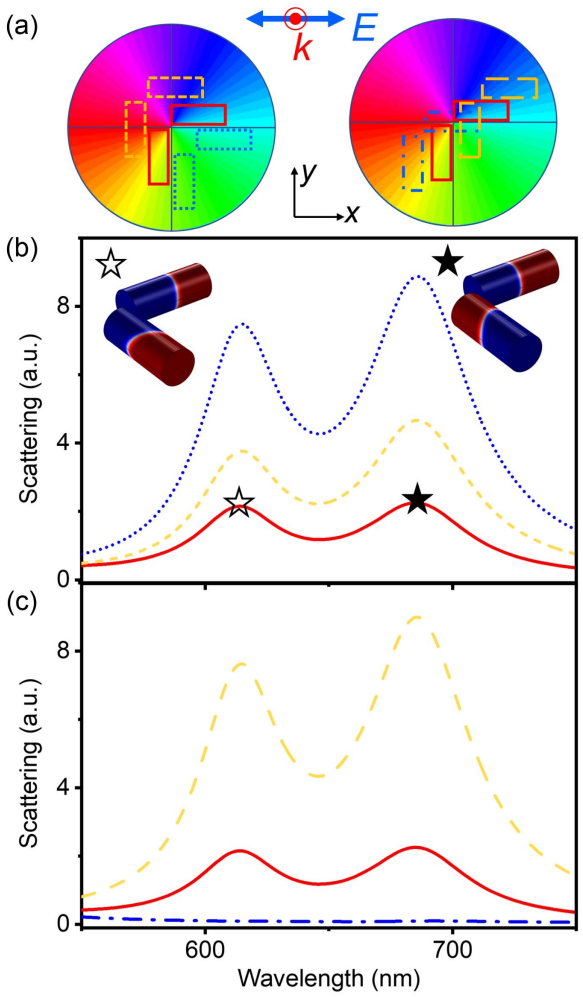

Fig. 5. Fano resonances by a pair of perpendicular nanorods under vortex beams. (a) Configurations of two perpendicular nanorods located at different positions of a vortex beam ($|\sigma, l\rangle$ equals $|0,1\rangle$). Optical scatterings of the vortex beam by this pair of perpendicular nanorods offset (b) in the second and fourth quadrants and (c) in the first and third quadrants. The insets in (b) show the surface charge distributions at the resonance peaks marked by the hollow and solid star symbols.

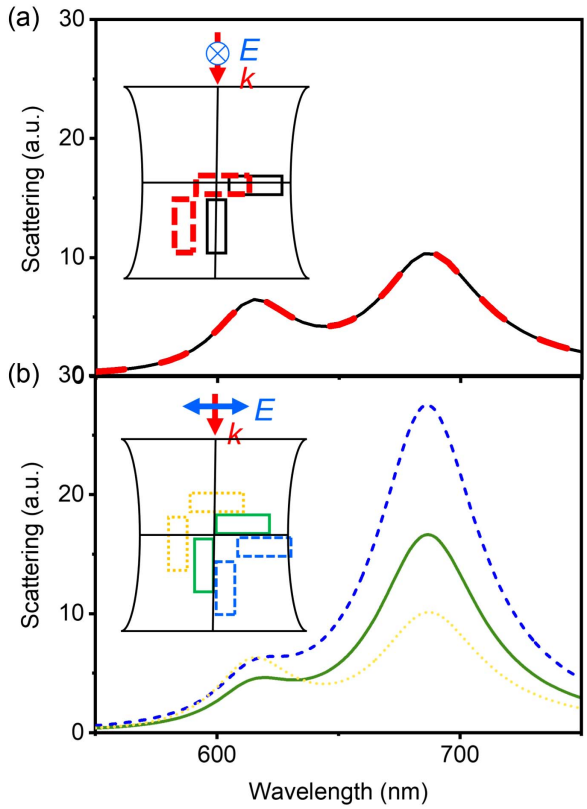

Fig. 6. Fano resonances by a dimer consisting of a horizontal nanorod and a vertical nanorod under a linearly polarized vortex beam ($l = 1$). Optical scatterings of the vortex beam by the dimer with one along the "vertical" light propagation direction and the other along the "horizontal" magnetic field (a) or electric field (b) direction. The insets show the locations of the dimer and the directions of the light propagation and electric field.

The peak intensities rely on how much the x-oriented nanorod is offset. The scattering spectrum shows the highest intensity when there is a largest offset, and the scattering disappears when the x-oriented nanorod is on-center, as shown by the blue line in Fig. 5(d).

Fano resonance can also happen to a dimer consisting of a vertical nanorod (along the light propagation direction) and a horizontal nanorod (along the electric field or magnetic field) under a linearly polarized vortex beam $|0,1\rangle$. The horizontal nanorod can be along the magnetic or electric field direction, as illustrated in the insets of Figs. 6(a) and 6(b). When the horizontal nanorod is along the magnetic field, Fano profile appears in the scattering spectrum, which hardly shows any difference when the dimer is moved around the beam center. The Fano resonance results from the interference between the bright mode of the vertical nanorod and the dark mode of the horizontal nanorod. The bright mode and dark mode are not influenced by the offset, so the Fano line shape does not change. When the horizontal nanorod is along the electric field, the Fano line shape changes with the offset of the dimer. This is because the horizontal nanorod is no longer a dark mode when it is offset. The longitudinal plasmon mode of the horizontal nanorod becomes stronger when it is more offset, so the Fano resonance gradually evolves into an in-phase coupling at the low energy state. The Fano resonance is highly tunable according to the location of the dimer.

3. CONCLUSION

In conclusion, we theoretically investigate the anomalous plasmon excitation and coupling behavior under vortex beams. For a single nanoparticle system, we reveal the interplay between OAM and SAM: when the nanoparticle is on-center, the nanoparticle polarization mode is determined both by OAM and SAM; when the nanoparticle is off-center, the nanoparticle polarization multiplicity is only determined by SAM, while OAM only puts a phase on the polarization. For an on-focal-plane nanodimer whose oscillation phases are controlled by OAM of light, we find anomalous plasmon coupling behaviors of an end-to-end anti-bounding high-energy mode and a

side-by-side bounding low-energy mode, which are exactly the opposite of the non-OAM case. In addition, we observe a contrary of the typical plasmonic Fano resonance in a nanorod dimer: one rod aligned with light propagation direction as the bright mode and the other aligned with light polarization direction as the dark mode. By controlling the location of the nanorod dimer, the couplings show high tunability from a Fano type to an in-phase coupling type, determined by how much the dark mode is excited. Our results offer insights into a fundamental question regarding the coupling of surface plasmons under a complex field. The plasmon behaviors enabled by OAM enrich the field of nanoplasmonics and have the potential to drive its continuous development and application.

APPENDIX A: METHODS

The simulations are performed using the Wave Optics Module of the software COMSOL Multiphysics. To simulate the plasmon behavior with OAM physical dimension, we adopt the two-step method [76]. First, simulate the background field distribution in the whole simulation area without nanoparticles. Second, obtain the total field, which is the superposition of the background field from the first step and the scattered field—a perturbation of the total field by the nanoparticles. The scattering intensities are obtained by integrating the far field $|E_{\mathrm{far}}|^2$ of the second step as

$$P_{\mathrm{scat}} = \sqrt{\frac{\epsilon_0}{\mu_0}} \oint_{S_{\mathrm{far}}} \mathrm{d}\tau |E_{\mathrm{far}}|^2, \tag{A1}$$

where the integration area S_{far} is a sphere with a radius of 1 m. Perfectly matched layers are used at the outermost boundaries. The dielectric functions of the gold nanorod are modeled by the Drude model [79]. In paraxial approximation, the LG field is written as

$$E(x,y,z) = \frac{1}{\sqrt{1+|m|^2}} \left[\hat{x} + m\hat{y} + \frac{-i}{k}\left(\frac{\partial}{\partial x} + m\frac{\partial}{\partial y}\right)\hat{z}\right] E_{\mathrm{pl}} e^{-ikz}, \tag{A2}$$

where SAM is described by complex number m with $\sigma = \frac{2\,\mathrm{Im}(m)}{1+|m|^2}$, and OAM is determined by the azimuthal quantum number l of an LG beam. σ equals ± 1 or 0, which stands for left, right circularly polarized or linearly polarized light, respectively. Additionally, there is a longitudinal electric field, E_z, which equals the partial derivatives of the transverse electric field with respect to x and y independently. The electric field E_{pl} of the LG beam is

$$E_{\mathrm{pl}} = \frac{w_0}{w(z)} \mathcal{L}_p^{|l|}\left[\frac{\sqrt{2}\rho}{w(z)}\right]^{|l|} \exp\left[\frac{-\rho^2}{w^2(z)} - \frac{ik\rho^2}{2R(z)} + i(2p+|l|+1)\arctan\left(\frac{z}{z_R}\right) - il\phi\right], \tag{A3}$$

where the wavefront curvature $R(z)$ is $\frac{z^2+z_R^2}{z}$, the Rayleigh range z_R is $\frac{\pi w_0^2}{\lambda}$, the spot radius $w(z)$ is $w_0\sqrt{1+(\frac{z}{z_R})^2}$, the waist radius w_0 is set to be 3000 nm unless otherwise stated, $\mathcal{L}_p^{|l|}(\xi)$ is the associated Laguerre polynomials as a function of $\frac{2\rho^2}{w^2(z)}$, and p and l are the topological charge numbers of the radial mode and azimuthal mode, respectively. The field distributions are visualized in Fig. 7 for better understanding the plasmon responses.

Funding. Ministry of Science and Technology of the People's Republic of China (2020YFA0211303); National

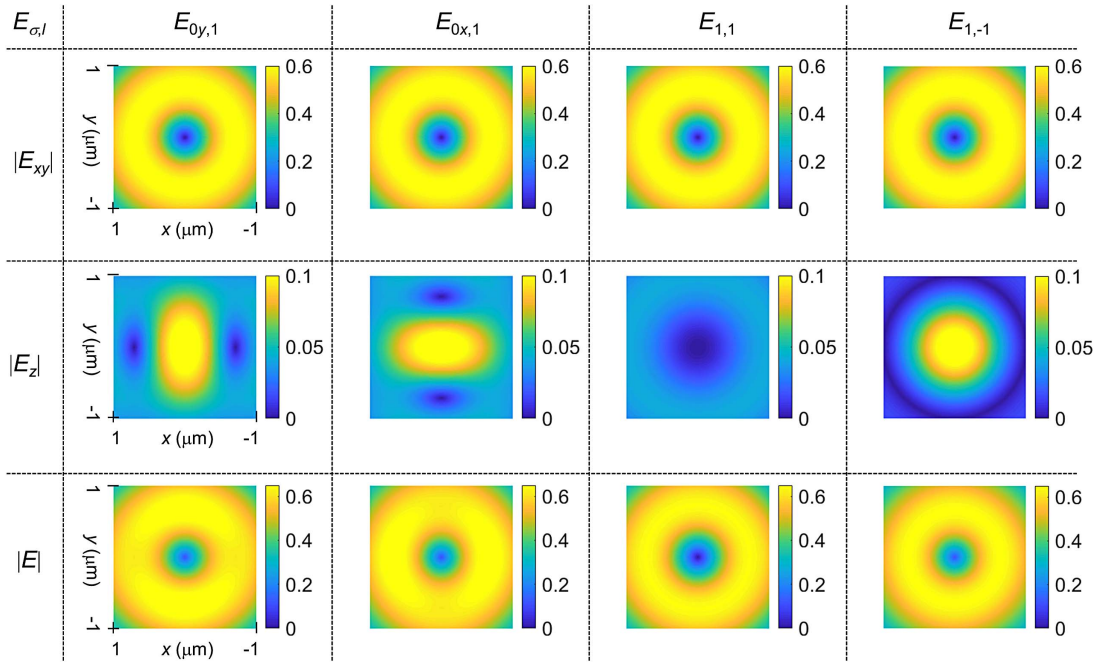

Fig. 7. E_{xy} (first row), E_z (second row), and amplitude $|E|$ (third row) on the focal plane of a y-polarized (first column), x-polarized (second column), right-circularly polarized (third column), and right-circularly polarized (fourth column) vortex beam of $l = 1$. The waist radius w_0 is 1000 nm, and other parameters are the same as explained in Appendix A.

Natural Science Foundation of China (11974108, 12074296, 12204169, 12211530044).

Disclosures. The authors declare no conflicts of interest.

Data Availability. Data underlying the results presented in this paper are not publicly available at this time but may be obtained from the authors upon reasonable request.

REFERENCES

1. S. A. Maier, *Plasmonics: Fundamentals and Applications* (Springer, 2007).
2. W. L. Barnes, A. Dereux, and T. W. Ebbesen, "Surface plasmon subwavelength optics," Nature **424**, 824–830 (2003).
3. P. Nordlander, "Plasmonics: the dark side of the ring," Nat. Nanotechnol. **8**, 76–77 (2013).
4. E. K. Payne, K. L. Shuford, S. Park, G. C. Schatz, and C. A. Mirkin, "Multipole plasmon resonances in gold nanorods," J. Phys. Chem. B **110**, 2150–2154 (2006).
5. S. Raza, S. Kadkhodazadeh, T. Christensen, M. Di Vece, M. Wubs, N. A. Mortensen, and N. Stenger, "Multipole plasmons and their disappearance in few-nanometre silver nanoparticles," Nat. Commun. **6**, 8788 (2015).
6. S. Linden, C. Enkrich, M. Wegener, J. Zhou, T. Koschny, and C. M. Soukoulis, "Magnetic response of metamaterials at 100 terahertz," Science **306**, 1351–1353 (2004).
7. C. Enkrich, M. Wegener, S. Linden, S. Burger, L. Zschiedrich, F. Schmidt, J. F. Zhou, T. Koschny, and C. M. Soukoulis, "Magnetic metamaterials at telecommunication and visible frequencies," Phys. Rev. Lett. **95**, 203901 (2005).
8. D. J. Yang, S. Zhang, S. J. Im, Q. Q. Wang, H. Xu, and S. Gao, "Analytical analysis of spectral sensitivity of plasmon resonances in a nanocavity," Nanoscale **11**, 10977–10983 (2019).
9. D. J. Yang, S. J. Ding, L. Ma, Q. X. Mu, and Q. Q. Wang, "SPP standing waves within plasmonic nanocavities," Opt. Express **30**, 44055–44070 (2022).
10. T. Kaelberer, V. A. Fedotov, N. Papasimakis, D. P. Tsai, and N. I. Zheludev, "Toroidal dipolar response in a metamaterial," Science **330**, 1510–1512 (2010).
11. H. S. Kang, W. Q. Zhao, T. Zhou, L. Ma, D. J. Yang, X. B. Chen, S. J. Ding, and Q. Q. Wang, "Toroidal dipole-modulated dipole-dipole double-resonance in colloidal gold rod-cup nanocrystals for improved SERS and second-harmonic generation," Nano Res. **15**, 9461–9469 (2022).
12. M. Hentschel, M. Schaferling, X. Duan, H. Giessen, and N. Liu, "Chiral plasmonics," Sci. Adv. **3**, e1602735 (2017).
13. J. Ni, S. Liu, G. Hu, Y. Hu, Z. Lao, J. Li, Q. Zhang, D. Wu, S. Dong, J. Chu, and C. W. Qiu, "Giant helical dichroism of single chiral nanostructures with photonic orbital angular momentum," ACS Nano **15**, 2893–2900 (2021).
14. C. Sonnichsen, B. M. Reinhard, J. Liphardt, and A. P. Alivisatos, "A molecular ruler based on plasmon coupling of single gold and silver nanoparticles," Nat. Biotechnol. **23**, 741–745 (2005).
15. T. H. Makaryan, "Numerical simulations on longitudinal surface plasmons of coupled gold nanorods," J. Contemp. Phys. **46**, 111–115 (2011).
16. E. Prodan, C. Radloff, N. J. Halas, and P. Nordlander, "A hybridization model for the plasmon response of complex nanostructures," Science **302**, 419–422 (2003).
17. P. Nordlander, C. Oubre, E. Prodan, K. Li, and M. I. Stockman, "Plasmon hybridization in nanoparticle dimers," Nano Lett. **4**, 899–903 (2004).
18. A. M. Funston, C. Novo, T. J. Davis, and P. Mulvaney, "Plasmon coupling of gold nanorods at short distances and in different geometries," Nano Lett. **9**, 1651–1658 (2009).
19. A. E. Miroshnichenko, S. Flach, and Y. S. Kivshar, "Fano resonances in nanoscale structures," Rev. Mod. Phys. **82**, 2257–2298 (2010).
20. B. Luk'yanchuk, N. I. Zheludev, S. A. Maier, N. J. Halas, P. Nordlander, H. Giessen, and C. T. Chong, "The Fano resonance in plasmonic nanostructures and metamaterials," Nat. Mater. **9**, 707–715 (2010).
21. Z.-J. Yang, Z.-H. Hao, H.-Q. Lin, and Q.-Q. Wang, "Plasmonic Fano resonances in metallic nanorod complexes," Nanoscale **6**, 4985–4997 (2014).
22. D.-J. Yang, Z.-J. Yang, Y.-Y. Li, L. Zhou, Z.-H. Hao, and Q.-Q. Wang, "Tunable Fano resonance in rod-ring plasmonic nanocavities," Plasmonics **10**, 263–269 (2014).
23. D. J. Yang, S. J. Im, G. M. Pan, S. J. Ding, Z. J. Yang, Z. H. Hao, L. Zhou, and Q. Q. Wang, "Magnetic Fano resonance-induced second-harmonic generation enhancement in plasmonic metamolecule rings," Nanoscale **9**, 6068–6075 (2017).
24. S. Zhang, D. A. Genov, Y. Wang, M. Liu, and X. Zhang, "Plasmon-induced transparency in metamaterials," Phys. Rev. Lett. **101**, 047401 (2008).
25. N. Liu, L. Langguth, T. Weiss, J. Kastel, M. Fleischhauer, T. Pfau, and H. Giessen, "Plasmonic analogue of electromagnetically induced transparency at the Drude damping limit," Nat. Mater. **8**, 758–762 (2009).
26. J. Zuloaga, E. Prodan, and P. Nordlander, "Quantum description of the plasmon resonances of a nanoparticle dimer," Nano Lett. **9**, 887–891 (2009).
27. O. Perez-Gonzalez, N. Zabala, A. G. Borisov, N. J. Halas, P. Nordlander, and J. Aizpurua, "Optical spectroscopy of conductive junctions in plasmonic cavities," Nano Lett. **10**, 3090–3095 (2010).
28. D. L. Andrews, *Structured Light and Its Applications: An Introduction to Phase-structured Beams and Nanoscale Optical Forces* (Academic, 2011).
29. N. M. Litchinitser, "Applied physics. Structured light meets structured matter," Science **337**, 1054–1055 (2012).
30. A. Forbes, "Structured light from lasers," Laser Photonics Rev. **13**, 1900140 (2019).
31. A. Forbes, M. de Oliveira, and M. R. Dennis, "Structured light," Nat. Photonics **15**, 253–262 (2021).
32. L. Allen, M. W. Beijersbergen, R. J. Spreeuw, and J. P. Woerdman, "Orbital angular momentum of light and the transformation of Laguerre-Gaussian laser modes," Phys. Rev. A **45**, 8185–8189 (1992).
33. Q. Zhan, "Cylindrical vector beams: from mathematical concepts to applications," Adv. Opt. Photonics **1**, 1–57 (2009).
34. Y. Shen, X. Wang, Z. Xie, C. Min, X. Fu, Q. Liu, M. Gong, and X. Yuan, "Optical vortices 30 years on: OAM manipulation from topological charge to multiple singularities," Light Sci. Appl. **8**, 90 (2019).
35. M. J. Padgett, "Orbital angular momentum 25 years on [Invited]," Opt. Express **25**, 11265–11274 (2017).
36. A. Aiello, P. Banzer, M. Neugebauer, and G. Leuchs, "From transverse angular momentum to photonic wheels," Nat. Photonics **9**, 789–795 (2015).
37. P. Banzer, M. Neugebauer, A. Aiello, C. Marquardt, N. Lindlein, T. Bauer, and G. Leuchs, "The photonic wheel - demonstration of a state of light with purely transverse angular momentum," J. Eur. Opt. Soc. Rap. **8**, 13032 (2013).
38. S. M. Barnett, "Optical angular-momentum flux," J. Opt. B **4**, S7–S16 (2002).
39. S. M. Barnett, M. Babiker, and M. J. Padgett, "Optical orbital angular momentum," Philos. Trans. R. Soc. A **375**, 20150444 (2017).
40. A. Chong, C. Wan, J. Chen, and Q. Zhan, "Generation of spatiotemporal optical vortices with controllable transverse orbital angular momentum," Nat. Photonics **14**, 350–354 (2020).
41. R. C. Devlin, A. Ambrosio, N. A. Rubin, J. P. B. Mueller, and F. Capasso, "Arbitrary spin-to-orbital angular momentum conversion of light," Science **358**, 896–901 (2017).
42. Z. Ji, W. Liu, S. Krylyuk, X. Fan, Z. Zhang, A. Pan, L. Feng, A. Davydov, and R. Agarwal, "Photocurrent detection of the orbital angular momentum of light," Science **368**, 763–767 (2020).
43. X. Fang, H. Ren, and M. Gu, "Orbital angular momentum holography for high-security encryption," Nat. Photonics **14**, 102–108 (2019).
44. A. E. Willner, Y. Ren, G. Xie, Y. Yan, L. Li, Z. Zhao, J. Wang, M. Tur, A. F. Molisch, and S. Ashrafi, "Recent advances in high-capacity free-space optical and radio-frequency communications using orbital

angular momentum multiplexing," Philos. Trans. R. Soc. A **375**, 20150439 (2017).
45. T. Stav, A. Faerman, E. Maguid, D. Oren, V. Kleiner, E. Hasman, and M. Segev, "Quantum entanglement of the spin and orbital angular momentum of photons using metamaterials," Science **361**, 1101–1104 (2018).
46. B. Chen, Y. Wei, T. Zhao, S. Liu, R. Su, B. Yao, Y. Yu, J. Liu, and X. Wang, "Bright solid-state sources for single photons with orbital angular momentum," Nat. Nanotechnol. **16**, 302–307 (2021).
47. X. Wang, Z. Nie, Y. Liang, J. Wang, T. Li, and B. Jia, "Recent advances on optical vortex generation," Nanophotonics **7**, 1533–1556 (2018).
48. Z. Zhang, X. Qiao, B. Midya, K. Liu, J. Sun, T. Wu, W. Liu, R. Agarwal, J. M. Jornet, S. Longhi, N. M. Litchinitser, and L. Feng, "Tunable topological charge vortex microlaser," Science **368**, 760–763 (2020).
49. A. Nicolas, L. Veissier, L. Giner, E. Giacobino, D. Maxein, and J. Laurat, "A quantum memory for orbital angular momentum photonic qubits," Nat. Photonics **8**, 234–238 (2014).
50. Y. Chen, S. Liu, Y. Lou, and J. Jing, "Orbital angular momentum multiplexed quantum dense coding," Phys. Rev. Lett. **127**, 093601 (2021).
51. S. W. Hancock, S. Zahedpour, and H. M. Milchberg, "Mode structure and orbital angular momentum of spatiotemporal optical vortex pulses," Phys. Rev. Lett. **127**, 193901 (2021).
52. K. Y. Bliokh, "Spatiotemporal vortex pulses: angular momenta and spin-orbit interaction," Phys. Rev. Lett. **126**, 243601 (2021).
53. X. Ouyang, Y. Xu, M. Xian, Z. Feng, L. Zhu, Y. Cao, S. Lan, B.-O. Guan, C.-W. Qiu, M. Gu, and X. Li, "Synthetic helical dichroism for six-dimensional optical orbital angular momentum multiplexing," Nat. Photonics **15**, 901–907 (2021).
54. N. Bozinovic, Y. Yue, Y. Ren, M. Tur, P. Kristensen, H. Huang, A. E. Willner, and S. Ramachandran, "Terabit-scale orbital angular momentum mode division multiplexing in fibers," Science **340**, 1545–1548 (2013).
55. H. Ren, X. Fang, J. Jang, J. Burger, J. Rho, and S. A. Maier, "Complex-amplitude metasurface-based orbital angular momentum holography in momentum space," Nat. Nanotechnol. **15**, 948–955 (2020).
56. H. Ren, X. Li, Q. Zhang, and M. Gu, "On-chip noninterference angular momentum multiplexing of broadband light," Science **352**, 805–809 (2016).
57. J. Wang, J.-Y. Yang, I. M. Fazal, N. Ahmed, Y. Yan, H. Huang, Y. Ren, Y. Yue, S. Dolinar, M. Tur, and A. E. Willner, "Terabit free-space data transmission employing orbital angular momentum multiplexing," Nat. Photonics **6**, 488–496 (2012).
58. H. Zhou, B. Sain, Y. Wang, C. Schlickriede, R. Zhao, X. Zhang, Q. Wei, X. Li, L. Huang, and T. Zentgraf, "Polarization-encrypted orbital angular momentum multiplexed metasurface holography," ACS Nano **14**, 5553–5559 (2020).
59. L. Deng, J. Deng, Z. Guan, J. Tao, Y. Chen, Y. Yang, D. Zhang, J. Tang, Z. Li, Z. Li, S. Yu, G. Zheng, H. Xu, C. W. Qiu, and S. Zhang, "Malus-metasurface-assisted polarization multiplexing," Light Sci. Appl. **9**, 101 (2020).
60. F. Tamburini, E. Mari, A. Sponselli, B. Thidé, A. Bianchini, and F. Romanato, "Encoding many channels on the same frequency through radio vorticity: first experimental test," New J. Phys. **14**, 033001 (2012).
61. K. Zhang, Y. Yuan, X. Ding, H. Li, B. Ratni, Q. Wu, J. Liu, S. N. Burokur, and J. Tan, "Polarization-engineered noninterleaved metasurface for integer and fractional orbital angular momentum multiplexing," Laser Photonics Rev. **15**, 2000351 (2020).
62. M. Fox, *Optical Properties of Solids* (Oxford University, 2002).
63. S. Franke-Arnold, "Optical angular momentum and atoms," Philos. Trans. R. Soc. A **375**, 20150435 (2017).
64. C. T. Schmiegelow and F. Schmidt-Kaler, "Light with orbital angular momentum interacting with trapped ions," Eur. Phys. J. D **66**, 157 (2012).
65. J. Weiner, P.-T. Ho, and K. C. Dee, *Light-matter Interaction: Fundamentals and Applications* (Wiley, 2003), Vol. **1**.
66. W. Frederick, *Optical Properties of Solids* (Academic, 2013).
67. N. B. Simpson, K. Dholakia, L. Allen, and M. J. Padgett, "Mechanical equivalence of spin and orbital angular momentum of light: an optical spanner," Opt. Lett. **22**, 52–54 (1997).
68. P. H. Jones, O. M. Maragò, and G. Volpe, *Optical Tweezers: Principles and Applications* (Cambridge University, 2015).
69. M. F. Andersen, C. Ryu, P. Clade, V. Natarajan, A. Vaziri, K. Helmerson, and W. D. Phillips, "Quantized rotation of atoms from photons with orbital angular momentum," Phys. Rev. Lett. **97**, 170406 (2006).
70. A. M. Yao and M. J. Padgett, "Orbital angular momentum: origins, behavior and applications," Adv. Opt. Photonics **3**, 161–204 (2011).
71. K. Sakai, K. Nomura, T. Yamamoto, and K. Sasaki, "Excitation of multipole plasmons by optical vortex beams," Sci. Rep. **5**, 8431 (2015).
72. T. Arikawa, T. Hiraoka, S. Morimoto, F. Blanchard, S. Tani, T. Tanaka, K. Sakai, H. Kitajima, K. Sasaki, and K. Tanaka, "Transfer of orbital angular momentum of light to plasmonic excitations in metamaterials," Sci. Adv. **6**, eaay1977 (2020).
73. R. M. Kerber, J. M. Fitzgerald, D. E. Reiter, S. S. Oh, and O. Hess, "Reading the orbital angular momentum of light using plasmonic nanoantennas," ACS Photonics **4**, 891–896 (2017).
74. D. K. Sharma, V. Kumar, A. B. Vasista, D. Paul, S. K. Chaubey, and G. V. P. Kumar, "Optical orbital angular momentum read-out using a self-assembled plasmonic nanowire," ACS Photonics **6**, 148–153 (2018).
75. R. Kerber, J. Fitzgerald, S. Oh, D. Reiter, and O. Hess, "Orbital angular momentum dichroism in nanoantennas," Commun. Phys. **1**, 87 (2018).
76. D. J. Yang, S. J. Im, Y. Li, C. S. Ri, K. S. Ho, J. S. Pae, and Q. Q. Wang, "Interactions between plasmonic nanoantennas and vortex beams," Nano Lett. **22**, 5015–5021 (2022).
77. S. Reich, N. S. Mueller, and M. Bubula, "Selection rules for structured light in nanooligomers and other nanosystems," ACS Photonics **7**, 1537–1550 (2020).
78. I. A. Litvin, N. S. Mueller, and S. Reich, "Selective excitation of localized surface plasmons by structured light," Opt. Express **28**, 24262–24274 (2020).
79. P. B. Johnson and R.-W. Christy, "Optical constants of the noble metals," Phys. Rev. B **6**, 4370–4379 (1972).